
Evolution of oxygen-metal electron transfer and metal electronic states during Mn-oxide catalyzed water oxidation revealed with *in situ* soft X-ray spectroscopy

Marc F. Tesch,^[a,b] Shannon A. Bonke,^[c,d] Travis E. Jones,^{*[e]} Maryam N. Shaker,^[a,f] Jie Xiao,^[a] Katarzyna Skorupska,^[b,e] Rik Mom,^[e] Jens Melder,^[g] Philipp Kurz,^[g] Axel Knop-Gericke,^[e] Robert Schlögl,^[b,e] Rosalie K. Hocking,^[h] and Alexandr N. Simonov^{*[c]}

Dedicated to Prof. Leone Spiccia – an outstanding scientist and personality who inspired this work.

Abstract: Manganese oxide (MnO_x) electrocatalysts are examined herein by *in situ* soft X-ray absorption spectroscopy (XAS) and resonant inelastic X-ray scattering (RIXS) during the oxidation of water buffered by borate (pH 9.2) at potentials from 0.75 to 2.25 V vs. the reversible hydrogen electrode. Correlation of L-edge XAS data with previous mechanistic studies indicates Mn^{IV} is the highest oxidation state involved in the catalytic mechanism. MnO_x is transformed into birnessite at 1.45 V and does not undergo further structural phase changes. At potentials beyond this transformation, RIXS spectra show progressive enhancement of charge transfer transitions from oxygen to manganese. Theoretical analysis of these data indicates increased hybridization of the Mn-O orbitals and withdrawal of electron density from the O ligand shell. *In situ* XAS experiments at the O K-edge provide complementary evidence for such a transition. This step is crucial for the formation of O₂ from water.

Electroreductive synthesis of fuels powered by renewable energy sources is globally recognized as a critical future technology needed to satisfy persistently surging energy demands. Such a synthesis requires an electron source of suitably large scale. An ideal option is water, the oxidation of which produces the electrons and protons that are necessary to synthesize fuels, as well as the useful by-product of O₂. In order to reach significant current densities at moderate overpotentials, the electrochemical water oxidation reaction requires the use of catalysts. Most of these are based on transition metal oxides of which manganese oxides/oxyhydroxides (MnO_x) are prominent examples. Although typically less active than catalysts based on the non-noble-metals nickel, iron or cobalt,^[1] manganese systems have advantages of abundance and lower toxicity. These considerations and inspiration from the biological catalyst for water-oxidation, the CaMn₄O_x cluster of the enzyme Photosystem II, have spurred great interest in MnO_x-catalyzed electrooxidation of H₂O for renewable fuel synthesis.^[2]

Remarkable progress in understanding the mechanistic aspects of water oxidation electrocatalysis has been achieved *via* three mutually complementary strategies: (i) density functional theory calculations to identify plausible reaction pathways,^[3] (ii) mechanistic kinetic studies for deciphering the mechanism,^[4] and (iii) spectroscopic analysis of catalytic materials to reveal transformations relevant to catalysis.^[5] For the latter, X-ray based techniques allowing comprehensive characterization of the structure and electronic properties of transition metal materials are of fundamental importance. A substantial body of valuable *ex situ* hard and soft X-ray spectroscopic studies on MnO_x-catalyzed water oxidation exists (see^[6] and refs therein). However, probing the states of metal oxides involved in different stages of the catalytic cycle requires *in situ* spectroscopic measurements under electrocatalytic conditions, which are limited in number for Mn-based catalysts.^[5a-d]

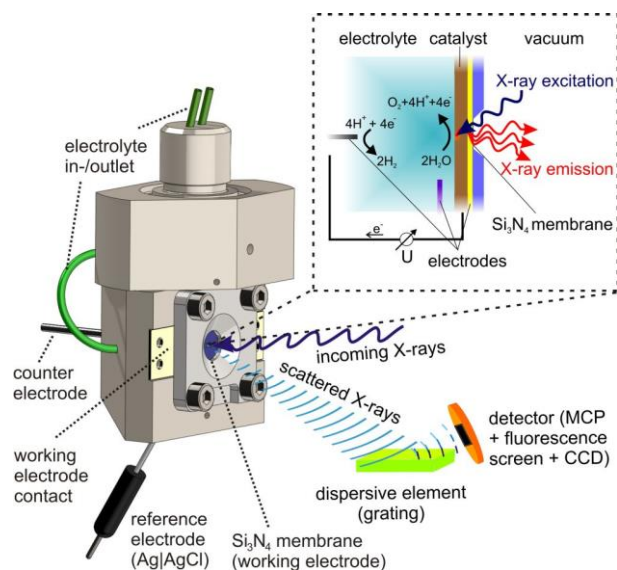
Hitherto, key *in situ* X-ray absorption spectroscopy (XAS) studies on MnO_x were undertaken at the Mn K-edge using hard X-rays, which is a powerful approach to decipher the structure and derive the average oxidation state of Mn. At the same time, significantly deeper insights into the electronic structure of the metal-ligand (Mn-O) sites and electronic transitions can be obtained *via* soft XAS and resonant inelastic X-ray scattering (RIXS) at the Mn L_{2,3}-edges. Thus, a comprehensive *in situ* soft XAS and RIXS study of MnO_x water oxidation catalysts is described herein. The spectra were collected with a wide range of potentials applied to the catalyst-modified electrodes, allowing changes in the state of

-
- [a] Dr. M. F. Tesch, M. N. Shaker, Dr. J. Xiao
Institut Methoden der Materialentwicklung
Helmholtz Zentrum Berlin für Materialien und Energie
Albert-Einstein-Straße 15, 12489 Berlin, Germany
- [b] Dr. M. F. Tesch, Dr. K. Skorupska, Prof. Dr. R. Schlögl
Abteilung Heterogene Reaktionen
Max-Planck-Institut für Chemische Energiekonversion
Stiftstraße 34-36, 45470, Mülheim an der Ruhr, Germany
- [c] Dr. S. A. Bonke, Dr. A. N. Simonov
School of Chemistry and the ARC Centre of Excellence for Electromaterials Science
Monash University
Victoria 3800, Australia
E-mail: alexandr.simonov@monash.edu
- [d] Dr. S. A. Bonke
Institut Nanospektroskopie
Helmholtz-Zentrum Berlin für Materialien und Energie
Kekuléstraße 5, 12489 Berlin, Germany
- [e] Dr. T. E. Jones, Dr. K. Skorupska, Dr. Rik Mom,
Dr. A. Knop-Gericke, Prof. Dr. R. Schlögl
Abteilung Anorganische Chemie
Fritz-Haber-Institut der Max-Planck-Gesellschaft
Faradayweg 4-6, 14195 Berlin, Germany
E-mail: trjones@fhi-berlin.mpg.de
- [f] Freie Universität Berlin
Fachbereich Physik
Arnimallee 14, 14159 Berlin, Germany
- [g] J. Melder, Prof. Dr. P. Kurz
Institut für Anorganische und Analytische Chemie and Freiburger
Materialforschungszentrum, Albert-Ludwigs-Universität Freiburg
Albertstraße 21, 79104 Freiburg, Germany.
- [h] Dr. R. K. Hocking
Department of Chemistry and Biotechnology,
Swinburne University of Technology,
John Street, Hawthorn, Victoria 3122, Australia

MnO_x to be correlated with the kinetics of the electrocatalytic reaction.

An equally important feature of the present work is the use of a fully parameterized model of MnO_x-catalyzed H₂O oxidation^[4] to define the potential needed to stabilize the catalyst in its putative active state (see Supporting Information (SI), Figure S1). Potentials examined in all previous studies were less positive than the critical value of ca 2 V vs. the reversible hydrogen electrode (RHE; all potentials are given vs. this reference hereinafter). Measurements at >2 V are needed to exclude or reveal the involvement of higher oxidation states of Mn in the catalytic mechanism of water electrooxidation.^[4]

To accommodate the requirements for a high-quality *in situ* L-edge XAS/RIXS electrochemical experiment, measurements were undertaken at the LiXEdrom end station of the BESSY II synchrotron facility using a custom-made flow cell (Scheme 1). Films of MnO_x were deposited by oxidative electrodeposition at an applied potential of 1.95 V on Au-coated Si₃N₄ membranes from aqueous Mn²⁺ solutions buffered with borate (0.1 M, pH 9.2). After deposition, a Mn-free borate buffer was used as a background electrolyte to obtain cyclic voltammograms and maintain the electrode at a constant potential during spectroscopic analysis. Further experimental details are provided in the SI.



Scheme 1. Schematic representation of the flow cell used for the *in situ* XAS and RIXS experiments. Incoming X-rays penetrate the 100 nm Si₃N₄ membrane and 20 nm Au layer, interact with the MnO_x catalyst and generate the emitted/scattered photons that are measured in an energy resolved fashion. MnO_x is in contact with an electrolyte solution. The potential applied to MnO_x/Au is controlled in a conventional three-electrode electrochemical configuration.

Figure 1 features representative cyclic voltammograms for the electrochemically deposited MnO_x in comparison to the unmodified Au-Si₃N₄ support, with both showing an expected combination of redox processes. On its own, the support exhibits features typical of gold electrodes, *viz.* surface oxide formation commencing at ca 1.3 V and subsequent reduction as a well-defined peak at ca 1.0 V. Functionalization of the electrode with

MnO_x suppresses these signals and produces a voltammetric curve dominated by processes associated with the water oxidation catalyst: (i) a combination of at least two redox transformations of Mn within the potential range 0.8-1.4 V^[4] and (ii) the electrocatalytic oxidation of H₂O at potentials >1.6 V. A mismatch between the anodic and cathodic counterparts of the voltammogram within this catalytic region is interpreted in terms of mass-transport limitations for the [H₂BO₃]/[B(OH)₄]⁻ conjugate base as defined by the experimental conditions employed, *viz.* no convection, comparatively low borate concentration, and a small solution volume.

In situ XAS/RIXS analysis was undertaken at nine potentials with special attention paid to the catalytic region (marked by dashed lines in Figure 1). The ground-state of the catalyst was probed with no potential applied after cyclic voltammetric analysis of freshly deposited MnO_x. XAS data were obtained in partial fluorescence yield (PFY) mode (Figure 2). We have also undertaken *ex situ* Mn L-edge XAS analysis in total electron yield (TEY) mode of as-deposited MnO_x and after conditioning at different potentials to confirm previous findings (Figure S2).^[5e] Both *in situ* PFY and *ex situ* TEY methods reveal typical multiplet structures at the Mn L₃ (ca 639-647 eV) and Mn L₂ (ca 650-657 eV) edges, stemming from transitions of the 2*p* core levels to the 3*d* conduction band (valence states) and subsequent relaxation *via* electron/photon emission.

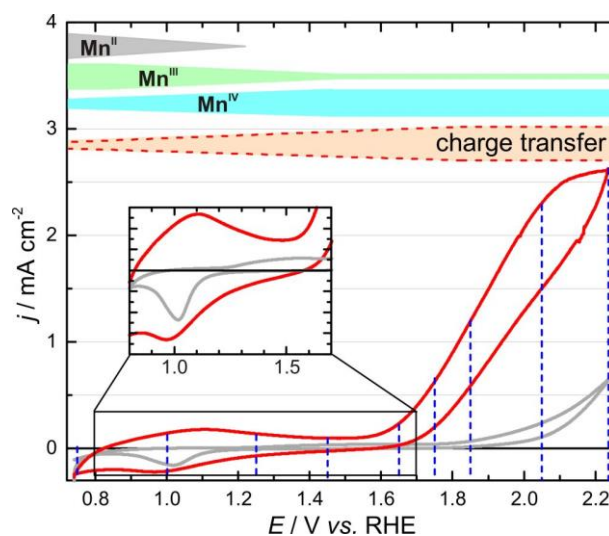


Figure 1. Cyclic voltammograms (scan rate 0.02 V s⁻¹) for electrodeposited MnO_x (red) and unmodified Au/Si₃N₄ (gray) in 0.1 M borate buffer (pH 9.2) at 23 ± 2 °C. The inset shows an enhanced plot of the outlined region. Bars with oxidation states illustrate the evolution of Mn oxidation states derived from spectroscopic data herein. Dashed lines show potentials used for *in situ* spectroscopic analysis. Currents are normalized to the geometric surface area of the electrode.

Application of increasingly positive potentials from 0.75 to 2.25 V induces significant changes to the shape of the XA spectra (Figure 2 and Figure S2). For the L₃ edge, peaks at 641.6 (mainly associated with Mn^{II}) and especially 640.2 eV (Mn^{II}) are increasingly suppressed, while the features at 640.8 and 643.7 eV (fingerprints of Mn^{IV}) notably enhance in intensity. At the L₂

edge, the whole multiplet shifts towards higher energies. The observed spectral changes are consistent with an increase of the formal Mn oxidation state at more positive potentials,^[7] and can be further correlated with structural transformations within the MnO_x catalyst films. The TEY data obtained for MnO_x are perfectly reproduced as a linear combination of the spectra for powder reference materials (Figure S4). However, Mn L-edge XAS is most sensitive to the differences in electronic states of the metal and might not provide unambiguous distinction between different phases in multicomponent materials. Hence, these data are mainly used herein to establish the effects of potential on the manganese oxidation state. On the basis of this type of analysis, the as-deposited MnO_x can be formally considered as a mixture of Mn₃O₄, Mn₂O₃ and birnessite in near equal amounts, which is oxidized to produce a material dominated by Mn₂O₃ and birnessite upon conditioning at 1.25 V. At 1.45 V and 1.75 V, the spectra of MnO_x strongly resemble those obtained for a birnessite standard, possibly with a minor contribution from MnO₂ (Figure S4), which accords with previous reports^[2a,5d,5e] and theoretical analysis (*vide infra*). Crucially, the TEY measurements were undertaken *ex situ* making it probable that the reactive species were reduced prior analysis. Importantly, the changes summarized above are reversible as confirmed by measurements undertaken with potentials switched in a random sequence.

When analysis is undertaken *in situ*, the PFY spectra contain features identical to those obtained in TEY mode (except for the well-known enhancement of the L₂-edge in FY^[8]) suggesting no X-ray beam damage to the samples, and the phase formed at positive potentials is therefore also identified as birnessite. The potential dependent evolution of the *in situ* spectra resembles the behavior observed in the *ex situ* experiments (*cf.* Figure 2 and Figure S2), but suggests deeper conversion to birnessite at less positive potentials. PFY is bulk sensitive (*ca* 10-100 nm), and strong signal changes upon oxidation of MnO_x attest to the complete transformation of the catalyst into birnessite. Upon oxidation at 1.75 V, the morphology of electrodeposited MnO_x also changed as detected by scanning electron microscopy (Figure S5); the initially present mixed flakes and grains were transformed into homogeneous flakes that more uniformly cover the support surface.

Thus, the data in Figure 2 infer that no significant changes to the oxidation state of MnO_x occur at potentials more positive than 1.45 V, as alterations in the shape and position of both the L₃ and L₂ multiplets are negligible. This observation is concordant with Mn K-edge XAS.^[5d] However, the catalyst became highly prone to X-ray induced damage whenever strongly oxidative potentials were applied, *viz.* >1.75 V (this was addressed by reducing the photon flux to enable collection of reliable spectroscopic data as explained in the SI). Moreover, this potential- plus X-ray-induced degradation produces Mn^{II} resonances in the XA spectra (Figure S6). This behavior is indicative of the generation of a highly reactive state of MnO_x at >1.75 V, which is readily reduced by X-rays into soluble species. It is important to emphasize that no beam damage was found during *in situ* measurements at ≤1.75 V at 10x higher X-ray intensity. Nevertheless, even L-edge XAS did not provide the necessary level of sensitivity to probe this labile MnO_x state, which incited us to undertake an *in situ* RIXS study.

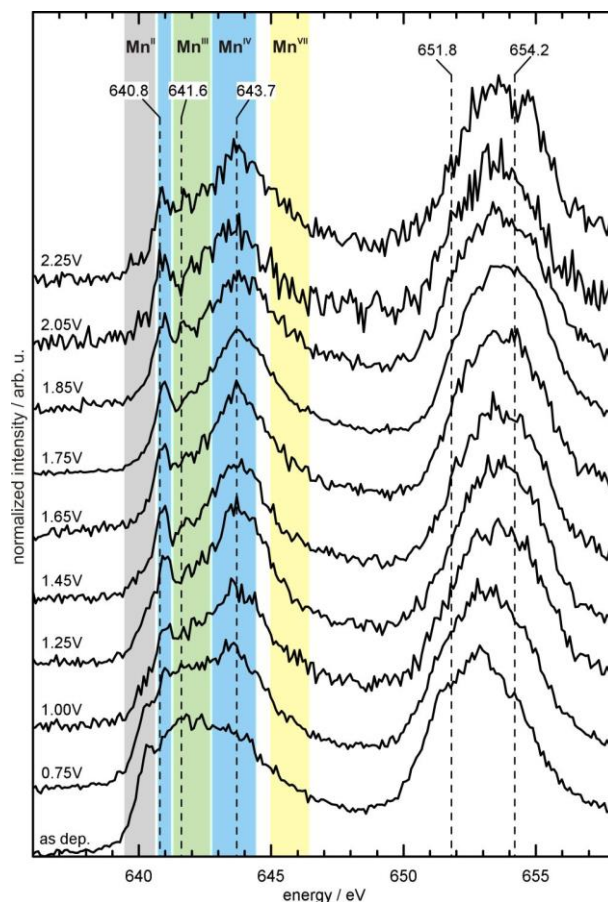


Figure 2. *In situ* absorption spectra at the Mn L_{2,3}-edges measured in PFY mode, *viz.* 2*p* → 3*d* transitions and subsequent photon emission by recombination, for MnO_x in borate buffer (0.1 M, pH 9.2) obtained after deposition with no potential applied (as dep.) and at the specified potentials reported vs. RHE. Dashed lines show energies used to collect RIXS spectra. Background shading shows the spectral regions prominently corresponding to particular Mn oxidation states.^[7] Corresponding current-time transients are exemplified in Figure S3. Data were obtained at 23 ± 2 °C and normalized to a maximum intensity of 1.

Figure 3 shows RIXS data obtained at different potentials (dashed lines in Figure 1) as energy loss spectra of scattered photons when irradiating the electrode with X-rays of a chosen energy (dashed lines in Figure 2). The energy uptake of the system due to inter- and intra-atomic electronic transitions can thus be probed. All spectra exhibit a peak from elastically scattered photons that did not transfer energy to the system, and hence appear at zero energy loss. Other spectral features result from an interplay of *dd* excitations and charge transfer transitions occurring at essentially constant energy loss independent of the excitation energy, as well as fluorescence features with positions that scale linearly with the excitation energy (for further details on the principles of RIXS see relevant reviews, *e.g.*^[9]). The need to employ low-intensity X-ray flux so as to avoid the photoreduction of Mn eventuated in a comparatively low RIXS signal to noise ratio. To compare the spectral features, a noise background signal was first subtracted from each spectrum and all spectra were subsequently normalized to an integrated intensity of 1 (see *Data Interpretation* section in the SI).

The energies used to record the RIXS data were chosen to cover the regions where the PFY spectra exhibited the most pronounced potential-induced changes (Figure 2), which reflect significant alterations in the electronic structure of the unoccupied states. Within the potential range examined, the RIXS spectra recorded at the Mn L_3 -edge (640.8, 641.6 and 643.7 eV) and the L_2 -edge (651.8 and 654.2 eV) exhibit prominent and clearly distinguishable features at 3-4 eV and 6-8 eV energy loss (Figure 3). The RIXS spectra at the L_2 -edge additionally develop new signals with energy losses above 10 eV that concertedly shift in position when changing the excitation energy (Figure 3). Such behavior is typical of fluorescence peaks.^[9]

The features appearing at constant energy loss, independent of the excitation energy, are typical of dd excitations (*ca* 1-5 eV), and charge transfer transitions (*ca* 5-10 eV). Interestingly, their energetic positions in the photon energy loss spectra are only marginally influenced by the applied potential (Figure 3). This observation suggests that the energies needed for a dd transition or a charge transfer are similar for all Mn oxidation states involved. Invariability in the position of the dd transition peak with the lowest energy loss at *ca* 3 eV indicates that the applied potentials do not induce a significant change in the band gap.

At the same time and most importantly, application of potential to the MnO_x films produces notable changes in the intensity of the charge transfer peaks (Figures 3 and S9). The strongest potential-induced effects are found in the RIXS spectra collected at low energies of the Mn L_3 -edge (640.8 and 641.6 eV). Specifically, the intensity of charge transfer features, which is low relative to the dd transition signals for the as-deposited state and at 0.75 V, progressively enhances as more positive potentials are applied. Deeper insights into this phenomenon were obtained *via* experiment-simulation comparisons.

Simulations of the XA spectrum of Mn^{IV} in a birnessite geometry were able to reproduce all experimentally observed features (Figure S10), thus verifying the appropriateness of the employed level of theory (full details of our approach based on a configuration interaction model are provided in the SI). Upon absorption of 640.8 eV photons, simulations support the excitation of electrons into Mn^{IV} σ (e_g) orbitals, which are empty for the $3d^8$ electronic configuration and octahedral geometry (Figure S11). Notably, simulations that do not account for orbital hybridization may produce XA spectra similar to those experimentally observed (Figure S12), but cannot reproduce the RIXS peaks at *ca* 5-10 eV (Figure S13). However, the simulated RIXS spectra show charge transfer features in the 5-10 eV range when accounting for orbital hybridization in the model (Figure S14), concordant with the experimental data and verifying the origin of these peaks. Specifically, theory indicates a ligand to metal charge transfer from an O $2p$ into a Mn $3d$ orbital. Considering crystal field theory and the octahedral geometry, electron transfer is expected to occur into the Mn σ (e_g) orbitals due to the two-fold greater orbital overlap compared to the π (t_{2g}) states. This is also supported in simulations by theoretically allowing or disallowing electron transfer into either the Mn σ or π orbitals (Figure S15).

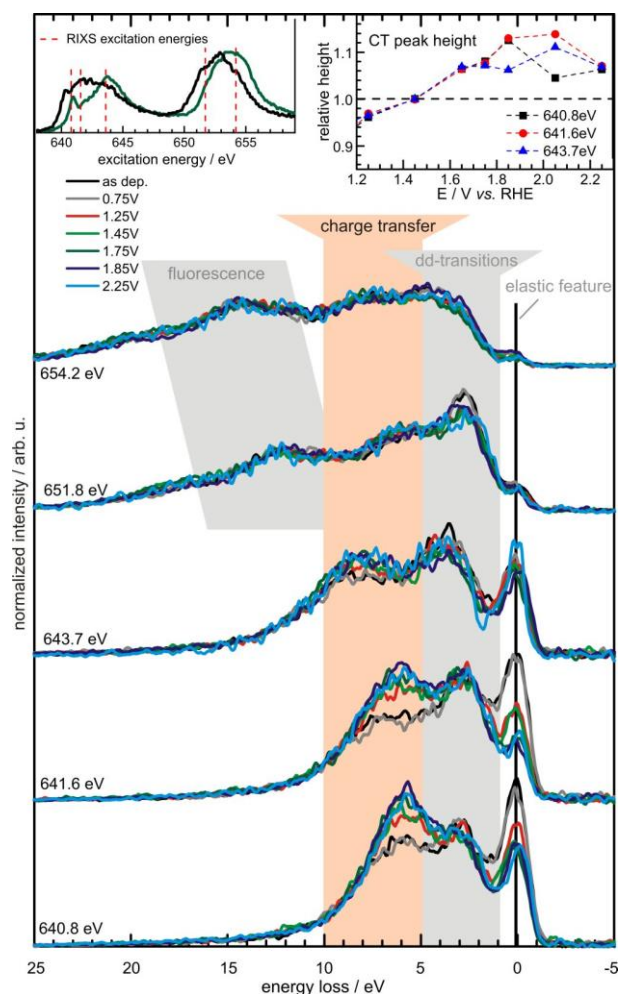


Figure 3. *In situ* energy loss spectra of scattered photons (RIXS) obtained at 23 ± 2 °C for MnO_x in 0.1 M borate buffer (pH 9.2) with no potential applied (black) and at 0.75 (gray), 1.25 (red), 1.45 (light green), 1.75 (dark green), 1.85 (dark blue), and 2.25 V vs. RHE (turquoise). Data were background corrected and normalized to an integrated intensity of 1. Energies of the incident X-rays were 640.8, 641.6, 643.7, 651.8 and 654.2 eV (relevant parts of the PFY spectra are shown in the left inset for as-deposited (black) and polarized at 1.75 V MnO_x (dark green)). Features of different origins discussed in the text are highlighted with background colors. The relative heights of the charge transfer (CT) features compared to the spectra taken at 1.45 V are shown in the right inset for the 640.8, 641.6, and 643.7 eV excitation energies. Data at all potentials examined (Figure S7), and a 2D RIXS map for MnO_x as-deposited and at 1.65 V (Figure S8), are shown in the SI.

The efficiency of charge transfer in first-row transition metal complexes is strongly linked to orbital hybridization,^[10] which was probed theoretically herein by varying the degree of hybridization of Mn $3d$ and O $2p$ orbitals. Within the framework of the employed model, this variation was achieved by altering the energy difference between the two orbitals (Δ), and the Mn-O bond length *via* the extent of orbital wavefunction overlap (the O-Mn hopping integral, V_{eg}). A decrease in Δ induces greater orbital hybridization, as does an increase in V_{eg} . Importantly, changes in these parameters had minimal effect on the simulated birnessite XA spectra (see Figure S10 and discussions in SI), consistent with the potential independent behavior of the experimental XAS data at >1.45 V (Figure 2). In contrast, the measured RIXS spectra

display clear intensity changes over this potential range (Figure 3), which can be mimicked by varying the degree of orbital hybridization in the simulations. Indeed, decreasing Δ increases the intensity of the charge transfer peaks, although this also shifts the peak position to lower energy loss, in disagreement with experimental observations (Figure S16). This is expected, as Δ defines the energy of the ligand to metal charge transfer. Meanwhile, higher V_{eg} also induces greater hybridization, but shifts the peak position in the opposite direction (Figure S17). Thus, the experimental observations can be simulated with a combination of these two parameters that both reflect enhanced hybridization, *viz.* a smaller energy difference between the Mn 3d and O 2p orbitals along with a Mn-O bond length contraction (Figure S18). The relative intensity of the charge transfer feature increased by 8-10% upon changing the applied potential from 1.45 to ≥ 1.75 V in the experimental spectra (Figure 3). This can be simulated using a heuristic approach by decreasing Δ on the order of an electron volt, combined with an increase in V_{eg} of a few hundred meV. These changes are indicative of a withdrawal of electron density from the O ligand shell (a comprehensive discussion is included in SI). This change in Δ can be ascribed to an increase of Mn 3d and O 2p orbital hybridization leading to significant ligand hole character, which would correspond to a formal oxidation state of -1 of the oxygen ligand ($d^4\bar{1}^1$), rather than O^{2-} ($d^3\bar{1}^0$).

The RIXS results reported herein correlate with prominent mechanistic proposals for water oxidation by the $CaMn_4O_x$ cluster in photosystem II,^[11] as well as *in situ* X-ray photoelectron spectroscopic and O K-edge XAS studies on IrO_2 electrocatalysts,^[12] with the generation of O^- species having been suggested to precede the O-O bond formation in both cases. Measurements at the O K-edge should also provide evidence for the O 2p hole formation detected by RIXS. This was achieved herein with the use of a setup that allows *in situ* XAS measurements in total electron yield mode (detailed description in the SI and schematic in Figure S19).^[12] The key feature of this setup is the separation of the working electrode from the solution with a Nafion membrane to provide a very thin layer of water through which photoelectrons can pass. Consequently, the *in situ* cell arrangements were very different for the RIXS and O K-edge measurements.

The use of the different cell layout (as shown in Figure S19) allowed chemically synthesized birnessite (SEM and XRD data in Figure S20) to be probed while enabling a measurable water electrooxidation rate (Figure S21a). Under these conditions, *in situ* XAS at the Mn L-edges confirmed that Mn oxidation states above IV are not formed (Figure S21b), which is consistent with results from the other *in situ* cell configuration (Figure 2). At the same time, the O K-edge spectra undergo continuous changes as more positive potentials are applied (Figure 4). Specifically, the resonance at 529 eV associated with transitions into locally unoccupied O 2p states hybridized with the lowest energy Mn 3d states (spin-majority e_g and t_{2g})^[12] enhance in intensity. At the same time, the resonance at 532 eV associated with oxidized graphene (Figure S21c) and O 2p states hybridized with the higher energy Mn states (spin-minority e_g)^[13] remains constant. Such behavior is indicative of a substantial increase in π covalency by donation of an electron from O^{2-} to a Mn^{IV} orbital (increased O 2p hole character in MnO_x). It is also similar to the

behavior of IrO_x during water oxidation catalysis.^[11] Crucially, this result is in full agreement with the aforesaid RIXS analysis. However, fundamental differences in the experimental conditions used for the two types of experiments do not allow direct quantitative correlations between them.

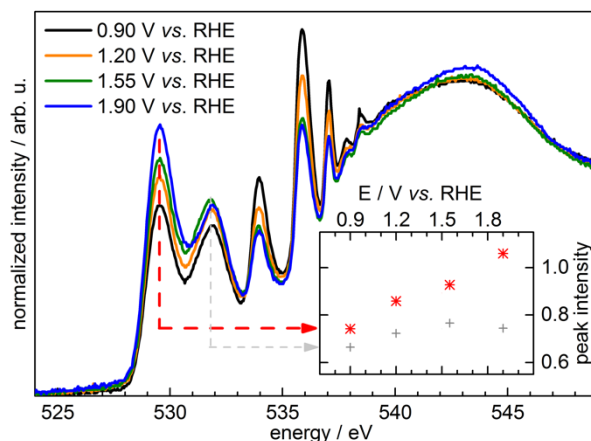


Figure 4. *In situ* O K-edge XA spectra obtained at 23 ± 2 °C for birnessite in contact with a Nafion membrane impregnated with 0.1 M phosphate buffer (pH 7.0) at 0.90 (gray), 1.20 (red), 1.55 (light green), and 1.90 V vs. RHE (dark blue). Inset shows the intensity at 529 and 532 eV as a function of potential. Data were recorded in the cell shown in Figure S19.

Finally, the RIXS/XAS spectroscopic data from the Mn L-edges can be directly linked to the mechanistic electrochemical study that guided the *in situ* analysis herein. To reiterate, XAS indicates that the highest Mn oxidation state of IV is reached at 1.45 V (Figure 2), whereas the RIXS charge transfer peak intensity increases until the application of 1.75 V (Figure 3). These saturation values correlate well with the potentials of redox processes for MnO_x electrocatalysts detected by Fourier transformed alternating current voltammetry.^[4] Therein, the last step for the oxidation of MnO_x prior to the onset of water oxidation occurs at ca 1.5 V and is not directly involved in catalysis. Based on the PFY spectra, this transition can now be related to the complete transformation of the catalyst into birnessite, which is the catalytically active phase of MnO_x . At the same time, the ac voltammetric signal directly coupled to the oxidation of H_2O is expected in the 1.70-1.75 V range (*cf.* water oxidation activity in Figure 1 and extrapolation of data in Figure 5b from Ref.^[4]), which is consistent with the stabilization of the RIXS data upon reaching these potentials (Figures 3 and S9). This indicates that MnO_x -catalyzed water oxidation requires facile charge transfer from O to Mn, which is achieved at ca 1.75 V and does not intensify with the application of more positive potentials (up to 2.25 V). Moreover, the aggregate of the XAS/RIXS data obtained herein and the outcomes of the preceding mechanistic study^[4] indicate that Mn^{IV} is the highest oxidation state involved in water oxidation electrocatalysis.

In summary, the present study demonstrates how *in situ* soft XAS and RIXS guided by comprehensive electrochemical analysis and supported by theoretical simulations consolidate into a truly powerful *modus operandi* for probing electrocatalytic mechanisms. Herein, this strategy was employed to investigate

water oxidation catalyzed by MnO_x under turnover conditions. It is demonstrated that: (i) birnessite is the catalytically active structural phase of MnO_x that does not undergo changes beyond ca 1.45 V; (ii) there is no evidence supporting involvement of manganese species with oxidation states higher than IV to the catalytic mechanism; and (iii) the degree of hybridization of Mn 3*d* and O 2*p* orbitals increases with positive potentials up to 1.75 V and thereby O-Mn charge transfer becomes increasingly facile. The latter potential correlates with the potential of the rate-determining electron transfer step.^[4] Importantly, the extent of orbital hybridization detected by *in situ* RIXS and quantified *via* theoretical simulations suggests that the ligand-metal charge transfer is associated with the formation of an O⁻ species. *In situ* O K-edge measurements verify the occurrence of this charge transfer. Thus, a crucial step in the interaction between an electrocatalyst and intermediates of water electrooxidation has been experimentally probed and correlated with the rate-determining electron transfer process.

Experimental Section

Full experimental details are provided in the Supporting Information.

Acknowledgements

The authors are grateful to Dr. R. Golnak for assistance during the XAS/RIXS synchrotron beamtime, Mr. I. Rudolph for Au-coating of the Si₃N₄ membranes, Mr. F. Siewert and Mrs. C. Klimm for microscopic characterization, Dr. C. Schwanke for assistance with the flow cell, Dr. K. Atak for scientific discussion related to theory and modeling, Prof. Dr. Anna Fischer for access to and assistance with the BMBF-funded HR-SEM at the ALU Freiburg (project EDELKAT, 03X5524), and Dr. A. Schnegg for support throughout the study. SAB and ANS acknowledge funding by the Australian Research Council *via* ACES (CE140100012); SAB acknowledges funding from the DFG through SPP 1601; MNS thanks the DAAD for the award of a doctoral scholarship (91527148); SAB and TEJ acknowledge the Alexander-von-Humboldt foundation for financial support; ANS is grateful to the Australian Synchrotron for funding through the International Synchrotron Access Program (ISP10692); MFT, KS, RM, JM, PK, AK-G and RS acknowledge financial support by the Federal Ministry of Education and Research (BMBF cluster project MANGAN, FKZ 03EK3545, 03SF0513 and 03SF0511A). We also thank Helmholtz-Zentrum Berlin and FHI for supporting the ISSS beamline at BESSY II.

Keywords: water electrooxidation • manganese oxide • RIXS • soft XAS • *in situ* spectroscopy

- [1] R. Subbaraman, D. Tripkovic, K.-C. Chang, D. Strmcnik, A. P. Paulikas, P. Hirunsit, M. Chan, J. Greeley, V. Stamenkovic, N. M. Markovic, *Nat Mater* **2012**, *11*, 550-557.
- [2] a) R. K. Hocking, R. Brimblecombe, L.-Y. Chang, A. Singh, M. H. Cheah, C. Glover, W. H. Casey, L. Spiccia, *Nat Chem* **2011**, *3*, 461-466; b) M. Wiechen, M. M. Najafpour, S. I. Allakhverdiev, L. Spiccia, *Energy Environ Sci* **2014**, *7*, 2203-2212.
- [3] a) I. C. Man, H.-Y. Su, F. Calle-Vallejo, H. A. Hansen, J. I. Martínez, N. G. Inoglu, J. Kitchin, T. F. Jaramillo, J. K. Nørskov, J. Rossmeisl, *ChemCatChem* **2011**, *3*, 1159-1165; b) H.-Y. Su, Y. Gorlin, I. C. Man, F. Calle-Vallejo, J. K. Nørskov, T. F. Jaramillo, J. Rossmeisl, *PCCP* **2012**, *14*, 14010-14022.
- [4] S. A. Bonke, A. M. Bond, L. Spiccia, A. N. Simonov, *J Am Chem Soc* **2016**, *138*, 16095-16104.
- [5] a) M. Yoshida, T. Yomogida, T. Mineo, K. Nitta, K. Kato, T. Masuda, H. Nitani, H. Abe, S. Takakusagi, T. Uruga, K. Asakura, K. Uosaki, H. Kondoh, *Chem Commun* **2013**, *49*, 7848-7850; b) Y. Gorlin, B. Lassalle-Kaiser, J. D. Benck, S. Gul, S. M. Webb, V. K. Yachandra, J. Yano, T. F. Jaramillo, *J Am Chem Soc* **2013**, *135*, 8525-8534; c) M. Yoshida, T. Yomogida, T. Mineo, K. Nitta, K. Kato, T. Masuda, H. Nitani, H. Abe, S. Takakusagi, T. Uruga, K. Asakura, K. Uosaki, H. Kondoh, *J Phys Chem C* **2014**, *118*, 24302-24309; d) I. Zaharieva, D. Gonzalez-Flores, B. Asfari, C. Pasquini, M. R. Mohammadi, K. Klingan, I. Zizak, S. Loos, P. Chernev, H. Dau, *Energy Environ Sci* **2016**, *9*, 2433-2443; e) M. Khan, E. Suljoti, A. Singh, S. A. Bonke, T. Brandenburg, K. Atak, R. Golnak, L. Spiccia, E. F. Aziz, *J Mater Chem A* **2014**, *2*, 18199-18203.
- [6] C. H. M. van Oversteeg, H. Q. Doan, F. M. F. de Groot, T. Cuk, *Chem Soc Rev* **2017**, *46*, 102-125.
- [7] L. A. J. Garvie, A. J. Craven, *Phys Chem Miner* **1994**, *21*, 191-206.
- [8] a) F.M.F. de Groot, M.A. Arrio, Ph. Sainctavit, Ch. Cartier, C.T. Chen, *Solid State Commun* **1994**, *92*, 991-995; b) R. Kurian, K. Kunnus, P. Wernet, S. M. Butorin, P. Glatzel, F. M. F. de Groot, *J Phys: Condens Matter* **2012**, *24*, 452201
- [9] L. J. P. Ament, M. van Veenendaal, T. P. Devereaux, J. P. Hill, J. van den Brink, *Rev Mod Phys* **2011**, *83*, 705-767.
- [10] M. N. Grisolia, J. Varignon, G. Sanchez-Santolino, A. Arora, S. Valencia, M. Varela, R. Abrudan, E. Weschke, E. Schierle, J. E. Rault, J. P. Rueff, A. Barthelemy, J. Santamaria, M. Bibes, *Nat Phys* **2016**, *12*, 484-492.
- [11] a) P. E. M. Siegbahn, *Acc Chem Res* **2009**, *42*, 1871-1880; b) L. Rapatskiy, N. Cox, A. Savitskiy, W. M. Ames, J. Sander, M. M. Nowaczyk, M. Rögner, A. Boussac, F. Neese, J. Messinger, W. Lubitz, *J Am Chem Soc* **2012**, *134*, 16619-16634; c) N. Cox, M. Retegan, F. Neese, D. A. Pantazis, A. Boussac, W. Lubitz, *Science* **2014**, *345*, 804.
- [12] a) V. Pfeifer, T. E. Jones, J. J. Velasco Velez, C. Massue, M. T. Greiner, R. Arrigo, D. Teschner, F. Girgsdies, M. Scherzer, J. Allan, M. Hashagen, G. Weinberg, S. Piccinin, M. Havecker, A. Knop-Gericke, R. Schlögl, *Phys Chem Chem Phys* **2016**, *18*, 2292-2296; b) V. Pfeifer, T. E. Jones, J. J. Velasco Velez, R. Arrigo, S. Piccinin, M. Havecker, A. Knop-Gericke, R. Schlögl, *Chem Sci* **2017**, *8*, 2143-2149.
- [13] F. M. F. de Groot, M. Grioni, and J. C. Fuggle, J. Ghijsen and G. A. Sawatzky, H. Petersen, *Phys. Rev. B* **1989**, *40*, 5715-5723.
